Lawrence Berkeley National Laboratory
Recent Work

Title
Spontaneous formation of highly periodic nano-ripples in inclined deposition of Mo/Si multilayers

Permalink
https://escholarship.org/uc/item/99k7k0hm

Journal
Journal of Applied Physics, 122(11)

ISSN
0021-8979

Authors
Voronov, DL
Gawlitza, P
Braun, S
et al.

Publication Date
2017-09-21

DOI
10.1063/1.4991377

Peer reviewed

eScholarship.org Powered by the California Digital Library
University of California

Spontaneous formation of highly periodic nano-ripples in inclined deposition of Mo/Si multilayers

D. L. Voronov, P. Gawlitza, S. Braun, and H. A. Padmore

Citation: Journal of Applied Physics **122**, 115303 (2017); doi: 10.1063/1.4991377
View online: http://dx.doi.org/10.1063/1.4991377
View Table of Contents: http://aip.scitation.org/toc/jap/122/11
Published by the American Institute of Physics

HIDEN ANALYTICAL
Instruments for Advanced Science


Gas Analysis
- dynamic measurement of reaction gas streams
- catalysis and thermal analysis
- molecular beam studies
- dissolved species probes
- fermentation, environmental and ecological studies


Surface Science
- UHV TPD
- SIMS
- end point detection in ion beam etch
- elemental imaging - surface mapping


Plasma Diagnostics
- plasma source characterization etch and deposition process reaction
- kinetic studies
- analysis of neutral and radical species


Vacuum Analysis
- partial pressure measurement and control of process gases
- reactive sputter process control
- vacuum diagnostics
- vacuum coating process monitoring

Contact Hiden Analytical for further details:
W www.HidenAnalytical.com
E info@hiden.co.uk
CLICK TO VIEW our product catalogue

Spontaneous formation of highly periodic nano-ripples in inclined deposition of Mo/Si multilayers

D. L. Voronov,[1,a)] P. Gawlitza,[2] S. Braun,[2] and H. A. Padmore[1]
[1]*Lawrence Berkeley National Laboratory, 1 Cyclotron Road, Berkeley, California 94720, USA*
[2]*Fraunhofer Institute for Material and Beam Technology, Winterbergstraße 28, 01277 Dresden, Germany*

(Received 20 June 2017; accepted 2 September 2017; published online 19 September 2017)

We investigated the growth of Mo/Si multilayers (ML) deposited using a highly collimated flux of ion-beam sputtered particles for a wide range of deposition angles. Growth of the multilayers at normal and moderately inclined deposition is dominated by surface relaxation resulting in smooth interfaces of the multilayer stack. The first signs of interface roughening are observed at a deposition angle of 45° with respect to the normal to the substrate surface. At an oblique angle of 55°, the ML interfaces undergo fast progressive roughening from the substrate to the top of the ML stack, leading to the formation of ripples which are perpendicular to the deposition flux direction. Deposition of the multilayer at an angle of 65° results in a highly periodic lateral ripple structure with a period of 10 nm. The mature ripple pattern forms during growth of only the first few layers and then stabilizes. The ripples propagate through the whole ML stack with almost no changes in frequency and amplitude, resulting in a highly periodic bulk array composed of silicon and molybdenum nano-rods closely packed in a 6-fold symmetric lattice. We present a simple model for the ripple growth, which gives results that are in good agreement with experimental data. *Published by AIP Publishing*. [http://dx.doi.org/10.1063/1.4991377]

I. INTRODUCTION

Multilayer (ML) coatings composed of dozens of nanometer thick alternating layers of high and low Z-materials are widely used in X-ray optics due to their high X-ray reflectivity. Multilayer-based optical components such as X-ray mirrors,[1,2] zone plates,[3,4] multilayer Laue lenses,[5] spectral purity filters,[6,7] and multilayer diffraction gratings[8–10] are of great importance for extreme ultraviolet (EUV) lithography, X-ray imaging, high resolution X-ray spectroscopy, and X-ray astronomy.

High performance in multilayer optics is achieved by careful optimization of the multilayer deposition process which aims to control layer growth in order to obtain sharp and smooth interfaces of the multilayer stack. It is relatively easy to achieve smooth interfaces when the deposition flux is normal to the surface of a plane or slightly curved substrate. Oblique deposition is usually avoided due to the risk of roughening of the interfaces due to shadowing effects. However, many advanced multilayer optic applications such as multilayer zone plates,[3,4] diffractive spectral purity filters,[11] and multilayer diffraction gratings[12–14] require the deposition of multilayers on highly curved or sculptured substrates which inevitably leads to oblique deposition geometry. For example, fabrication of multilayer blazed gratings (MBGs) for EUV and soft X-ray wavelengths requires deposition of multilayers on a saw-tooth substrate with highly faceted surfaces resulting in high local angles between the direction of the deposition flux and the surface. Growth of multilayers under such conditions has not been studied systematically, and growth fundamentals are not well understood. A better understanding of processes which control ML growth under inclined deposition conditions is required to achieve further progress in advanced multilayer optic performance. Moreover, the angle of deposition might be an additional leverage to control the ML growth on sculptured substrates. In this work, we investigate the growth of Mo/Si multilayers deposited using an ion-beam sputtering method for a wide range of deposition angles. We report on a very unusual growth regime which occurs for inclined deposited multilayers, and which results in a highly periodic lateral structure of the ML interfaces. In addition, we present a model for this newly discovered growth regime.

II. EXPERIMENT

In this work, we chose ion-beam sputtering as a ML deposition technique since it provides two important advantages for the systematic investigation of inclined multilayer growth. First, ion-beam sputtering allows a well-defined and a highly collimated atomic flux required for accurate control of the deposition angle (Fig. 1). Due to the large distance of 530 mm from the 80 mm wide target to the substrate, the residual divergence of the deposition flux on the substrate was small (7°). The deposition on laterally translated substrates was performed through a 43 mm wide aperture, so that the maximum possible variation of the deposition angle on the substrate did not exceed ±7°. Second, the deposition was performed in a high vacuum chamber (10^{-5} mTorr), which minimized atomic collisions and preserved a relatively high energy of about 10 eV of the sputtered atoms on their way towards the substrate. Note that magnetron sputtering can generate particles of same energy, but they are expected to thermalize on their travel to a remote substrate for a typical pressure of 10^{-3} mTorr of the sputtering gas.

a)E-mail: dlvoronov@lbl.gov

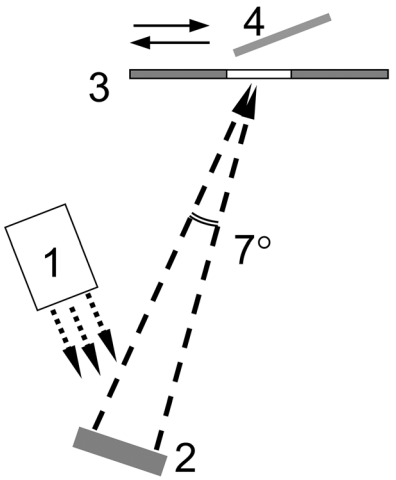

FIG. 1. Schematic of the ion-beam sputtering deposition setup: 1—ion gun, 2—target, 3—aperture, 4—substrate.

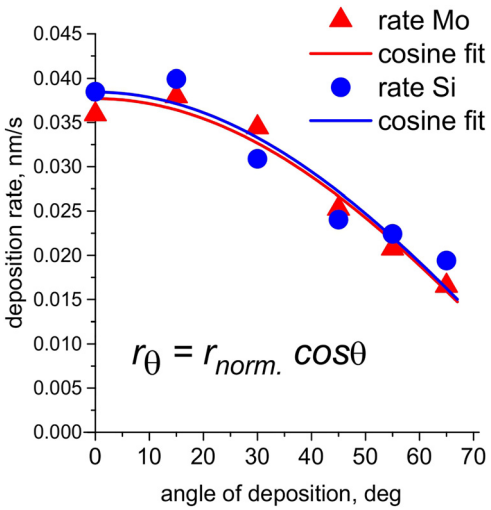

FIG. 2. Dependence of deposition rates of Mo and Si (red and blue symbols) on the angle of deposition. Cosine fits are shown with the red and blue curves, respectively.

The energy brought to the substrate surface by the deposition flux is expected to promote substantial mobility of atoms on the growing surface as compared to lower energy deposition techniques such as thermal or e-beam evaporation and magnetron sputtering widely used for ML fabrication.

The multilayers were deposited on superpolished silicon single crystal substrates. The surface of the substrates was cleaned by 500 eV Ar^+ ion-beam prior to the deposition. The sputtering resulted in a few nanometer thick amorphous surface layer of the silicon substrate.

Kr^+ ions of energy of 300 eV were used to sputter Mo and Si targets. The choice of heavy particles of relatively low energy as sputtering species was aimed to minimize the probability of recoil of the sputtering ions from the target and avoid re-sputtering growing films by the recoiled Kr neutrals.

Periodic Mo/Si multilayers were deposited at the angles of 0°–65° between the deposition flux and the normal to the surface of the plane Si substrates. The multilayers consisted of 50 bi-layers. The ML growth started with the deposition of a Mo layer, and the topmost layer was capped in Si for all the multilayers. X-ray reflectometry was used to measure the bilayer thickness (d-spacing) of the periodic multilayers to calibrate the deposition rates. Deposition rates for different angles of deposition were found to follow the classical cosine law (Fig. 2). The deposition time was calibrated accordingly for different deposition angles to provide the goal d-spacing of 6.7 nm for all the multilayers. The morphology of the top surface of multilayers was investigated by atomic force microscopy (AFM). The internal structure of multilayers was studied using cross-sectional transmission electron microscopy (TEM).

III. RESULTS

AFM images of the top surface of the multilayers deposited at angles of 0°, 15°, 30°, 45°, 55°, and 65° are shown in Fig. 3. The multilayer deposited at normal incidence has a very smooth surface with a residual roughness of 0.11 nm rms [Fig. 3(a)]. A highly smooth surface of similar morphology is observed for moderate deposition angles of 15° and 30° [Figs. 3(b) and 3(c)]. At an angle of 45°, the planar morphology of the surface starts to change exhibiting the appearance of small surface bumps elongated in the direction perpendicular to the incident deposition flux, which is accompanied by an increase of the surface roughness to 0.16 nm rms [Fig. 3(d)]. Further increase of the angle of deposition results in dramatic changes in surface morphology. At an angle of 55°, a pronounced ripple structure is observed [Fig. 3(e)]. The ripples with a characteristic wavelength of 20 nm and an amplitude of a few nanometers are oriented perpendicular to the direction of the deposition flux. The density of the ripple pattern tends to increase with the deposition angle. A ripple pattern with twice the density forms at a deposition angle of 65° [Fig. 3(f)]. The power spectral density (PSD) of the surface exhibits a pronounced peak at a spatial frequency of 0.1 nm^{-1} [red curve in Fig. 4(a)] showing long range ordering of the surface ripples. Note that the ripple peak is located on the inclined part of the PSD curve, i.e., the ripple frequency is much higher than the transition frequency of 0.01 nm^{-1} which corresponds to the correlation length of the surface. This is a very uncommon behavior as compared to the usually observed PSD spectra of smooth or rough multilayers [see black and blue curves in Fig. 4(a)], which consist of a frequency independent horizontal part and a frequency dependent slope part. According to the existing growth models,[15,16] surface relaxation is supposed to dominate at distances shorter than the correlation length, L, and any roughening at frequencies higher than 1/L should not be possible.

Cross-sectional TEM images in Figs. 5–7 reveal the internal structure of the multilayers and give an insight into the time evolution of the growing surface and ripple formation. Mo/Si multilayers deposited at angles varying between 0° and 45° show a similar structure dominated by smooth layers with some diffusional intermixing of materials at the interfaces [Figs. 5(a)–5(c)] that is well known from the literature.[17] Some minor roughening of the interfaces is observed for the upper layers of the 45° multilayer [Figs. 5(d) and 5(e)], which is in agreement with the AFM measurements [Fig. 3(d)].

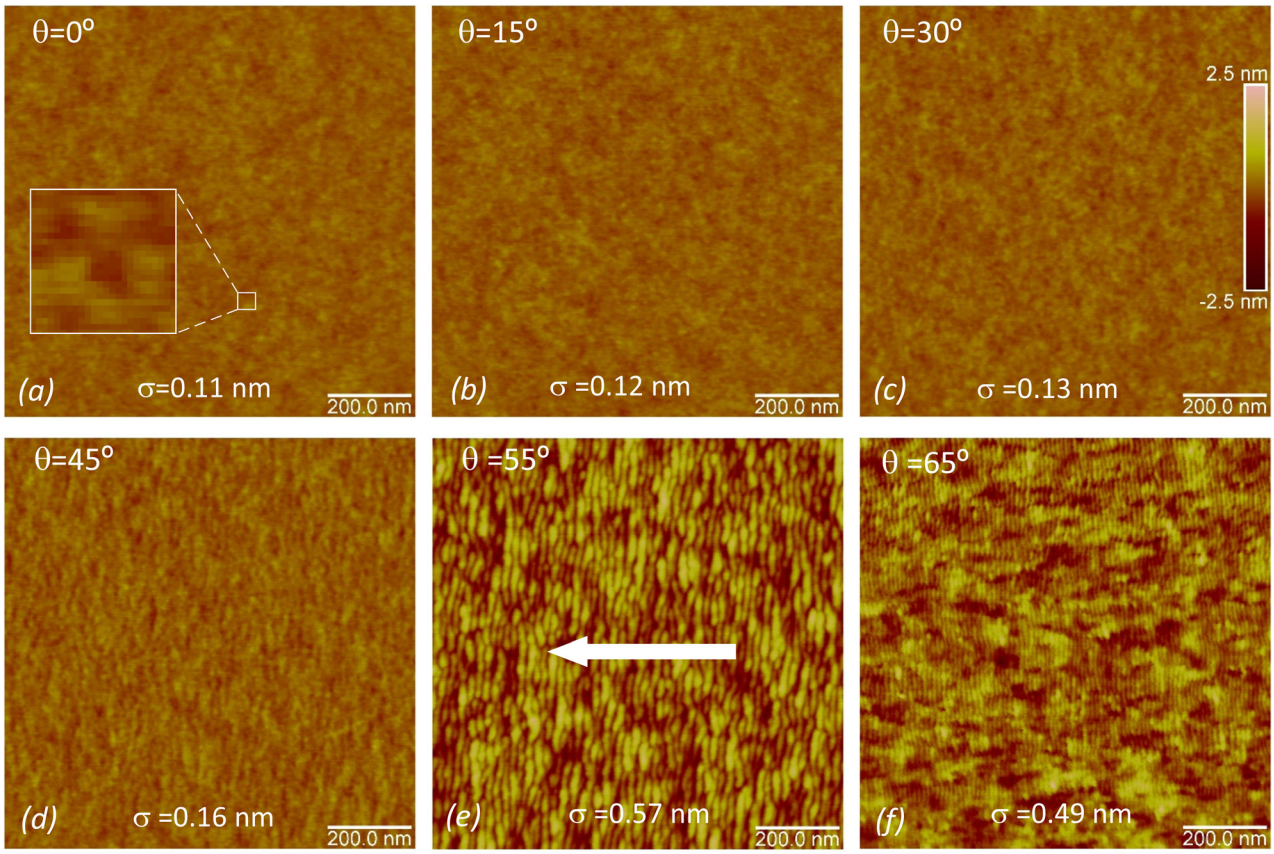

FIG. 3. AFM images of the top surface of ion-beam sputtered Mo/Si multilayers deposited at the angles of 0°–65° [(a)–(f)]. Projection of the deposition flux on the substrate surface is shown with an arrow for the 55° sample.

The structure of the multilayer deposited at an angle of 55° [Fig. 6(a)] is dramatically different from depositions performed at lower angles. Initially smooth interfaces near the substrate [Fig. 7(a)] undergo gradual roughening, which progressively increases from the substrate towards the top surface and results in the formation of ripples [Fig. 7(b)]. The ripples are replicated by the following layers and propagate through the whole multilayer stack with an apparent angle of 45°. As the amplitude of the ripples increases, they trigger shadowing effects as observed in the upper part of the multilayer stack [Fig. 6(a)]. Such growth behavior of the multilayer resembles columnar growth.[18,19] There is, however, a substantial difference in the deposition conditions and the structure of the multilayer from the classical columnar structure. Typically, columnar growth of MLs is observed when surface relaxation is substantially suppressed,[18,21] which is not the case for the multilayers considered in this work. High surface adatom mobility inherent to the ion-beam sputtered multilayers causes effective smoothing of the surface in the transverse direction resulting in the formation of ripples as opposed to bumps of the column structure.[18,19,21] Due to the ripple growth, the final structure of coating consists of two-dimensional slabs rather than one-dimensional columns/pillars: compare the rippled surface of the 55° multilayer [Fig. 3(e)] to a bumpy surface [Fig. 4(b)] of a Mo/Si multilayer grown under low surface relaxation conditions that exhibits a typical column structure (see details in Ref. 21). Diffraction of electrons on the system of slanted parallel slabs results in extra reflections observed in low angle diffraction patterns [see the inset in Fig. 6(a)]. Since the lateral dimension of the slabs varies in some range, the extra reflections form elongated spikes around the primary reflections caused by the periodic structure of the multilayer.

Multilayers deposited at an angle of 65° exhibit a remarkably ordered array structure [Fig. 6(b)], which, to our knowledge, has never been reported. The ripples of a very short wavelength of 7–8 nm develop within the few first layers. Some minor coarsening of the ripples occurs within the following few layers, and then the ripple period stabilizes at 10 nm (Fig. 8). The pronounced in-plane periodicity of the ripples combined with the vertical periodicity of the multilayer stack results in a two-dimensional periodicity of the array composed of Si and Mo nano-rods, which are perpendicular to the TEM image plane [Fig. 7(d)]. Low-angle electron diffraction exhibiting distinct reflections resembling ones for single crystals [see the inset in Fig. 6(b)] confirms the long range periodicity of the 6-fold symmetric array.

The TEM image in Fig. 7(c) shows the initial stages of ripple formation. The 1st molybdenum layer of the coating is grown on the amorphous Si layer formed during the ion-beam treatment of the single crystal substrate prior to the deposition (see Experiment, Sec. II). The interface between the substrate and the 1st Mo layer [denoted as #0 in Fig. 7(c)] is very smooth, which indicates that the ion-beam cleaning did not roughen the substrate, and the film grew on a very smooth surface. The top surface of the 1st Mo layer is

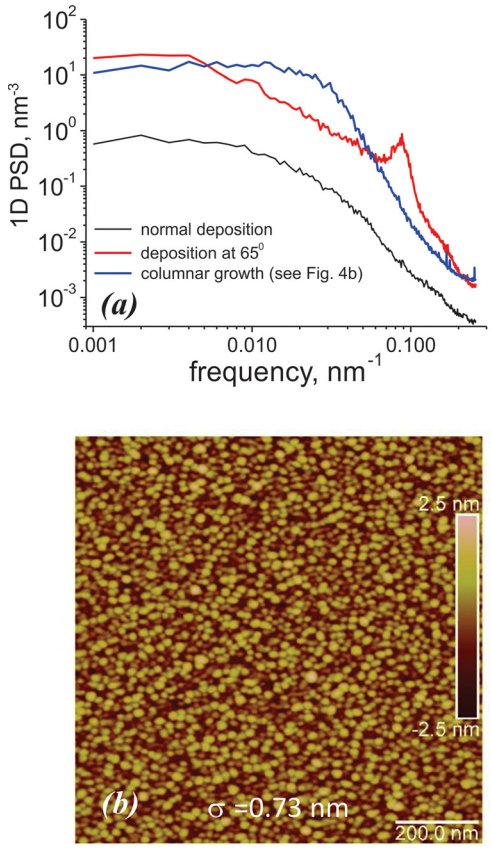

FIG. 4. PSD spectra of the top surface of the normally deposited multilayer (black curve) and the multilayer deposited at an angle of 65° (red curve) calculated across the ripples (a). The blue curve shows the PSD spectrum of a rough Mo/Si multilayer (see details in the text and in Ref. 21). AFM image of the rough multilayer (b).

fairly smooth, although some minor stochastic roughening is observed [compare Si-on-Mo interfaces denoted as #1 in Figs. 7(a) and 7(c)]. The subsequent interfaces exhibit, on one hand, a drastic increase of the roughness amplitude and, on the other hand, a transition from random roughening to selective enhancement of a surface mode of a defined spatial frequency. The morphology of the Mo-on-Si interface #2 in Fig. 7(c) is distinctly dominated by a spatial wavelength of about 7 nm. The resonance frequency becomes even more pronounced for the following interfaces #3 and #4, resulting in the formation of a highly periodic ripple structure. Formation of elongated slanted voids which appear as light streaks between the ripples on the upper part of the TEM image in Fig. 7(c) indicates that strong shadowing comes into play, and a transition from the continuous rippled film to an array of isolated columns/slabs occurs. The slabs inherit the very well-defined periodicity of the ripples and have almost the same height and width throughout the whole multilayer stack (Figs. 6(b) and 8). Such highly ordered surface structures have never been reported for columnar growth, where the competitive growth of pillars of different size results in the suppression of more shadowed areas and growth, and the lateral expansion of less shadowed pillars results in surface coarsening with film thickness.[18–21] Some coarsening of the ripples observed for the 55° multilayer [Fig. 6(a)] might be interpreted as slower development of the resonance frequency of the ripples. Indeed, Fig. 8 shows a trend of stabilization of the ripple/slab wavelength of 20 nm for the upper layers, and they exhibit a well-ordered ripple structure shown in Fig. 7(b) similar to the 65° multilayer.

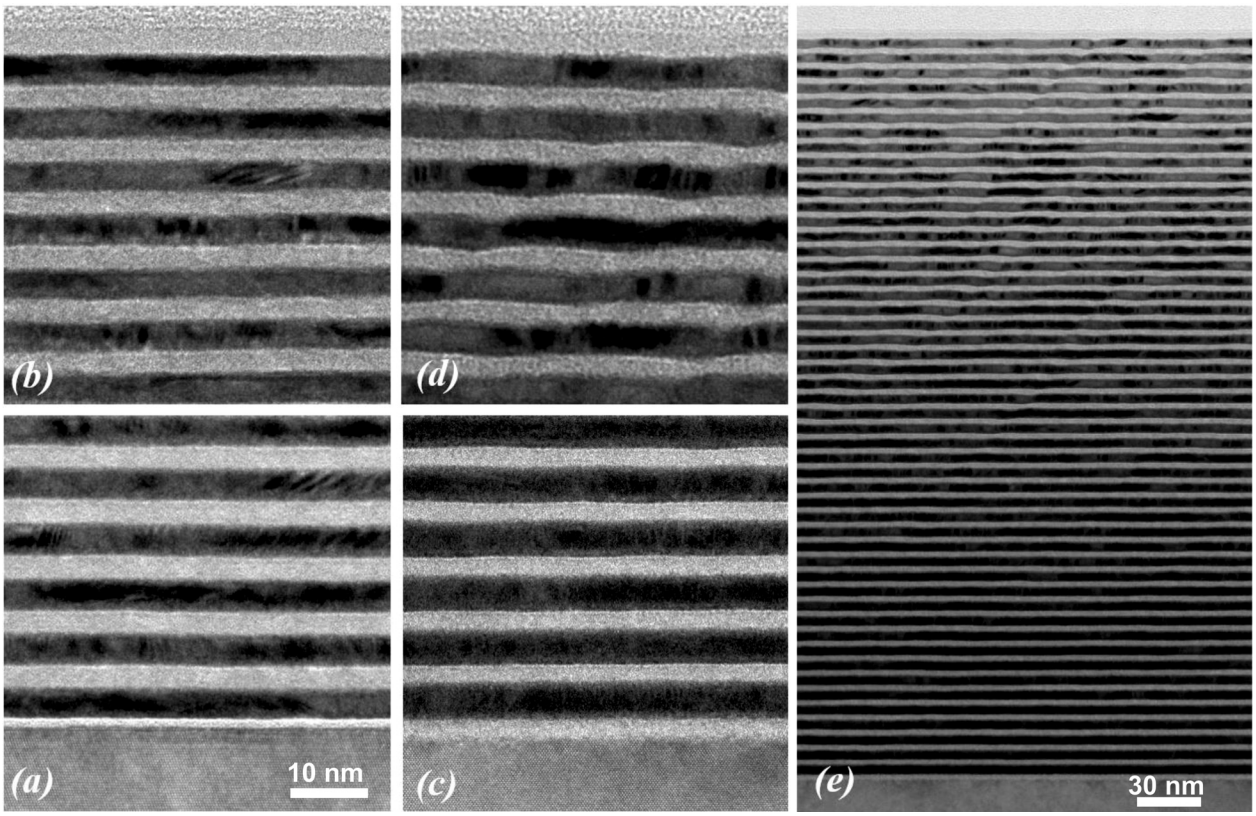

FIG. 5. High resolution TEM images of the bottom [(a) and (c)] and upper [(b) and (d)] layers of the multilayers deposited at 0° [(a) and (b)] and 45° [(c), (d), and (e)].

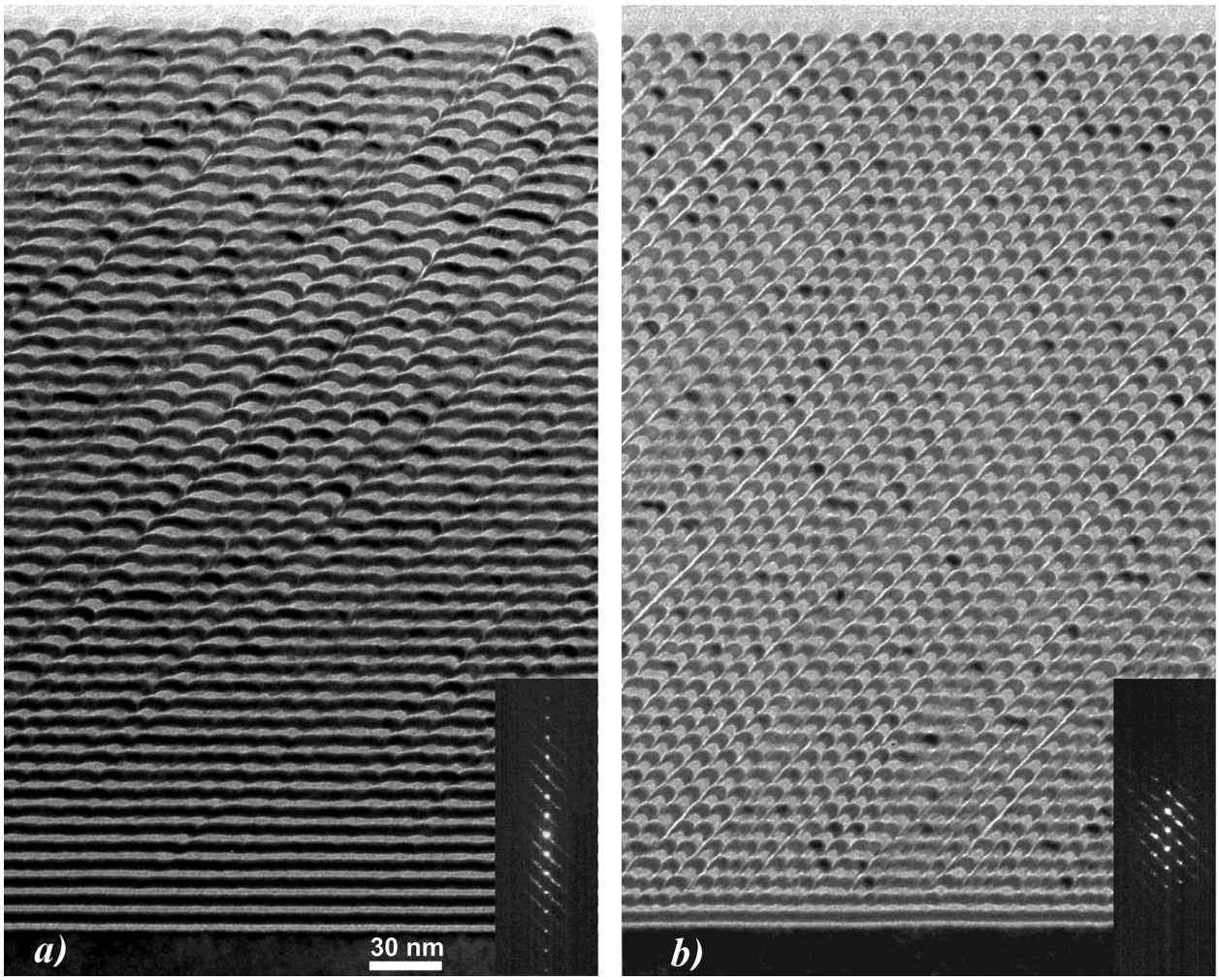

FIG. 6. Cross-section TEM images of the Mo/Si multilayers deposited at the angles of 55° (a) and 65° (b). The insets show small angle electron diffraction patterns.

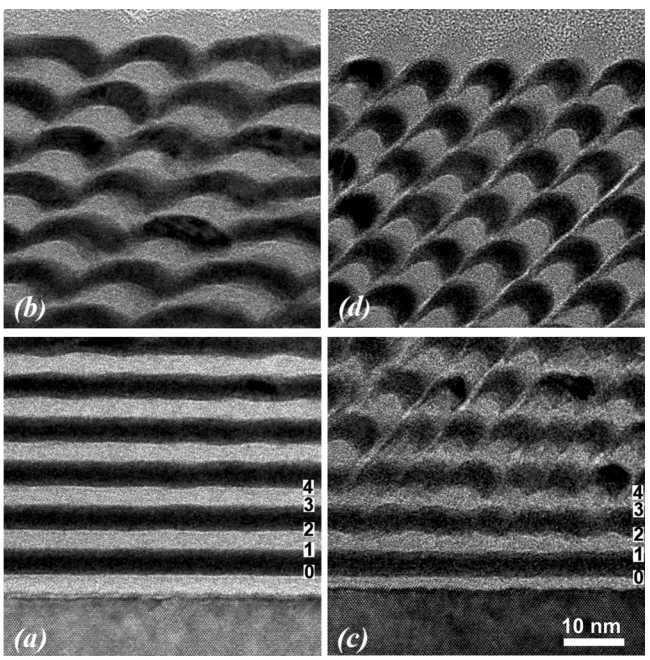

FIG. 7. High resolution TEM images of the bottom [(a) and (b)] and upper [(c) and (d)] layers of the multilayers deposited at 55° [(a) and (b)] and 65° [(c) and (d)].

IV. DISCUSSION

A. Ripples and columnar growth

The inclined deposited multilayers exhibit strong roughening of the interfaces, and the slab structure of the multilayers

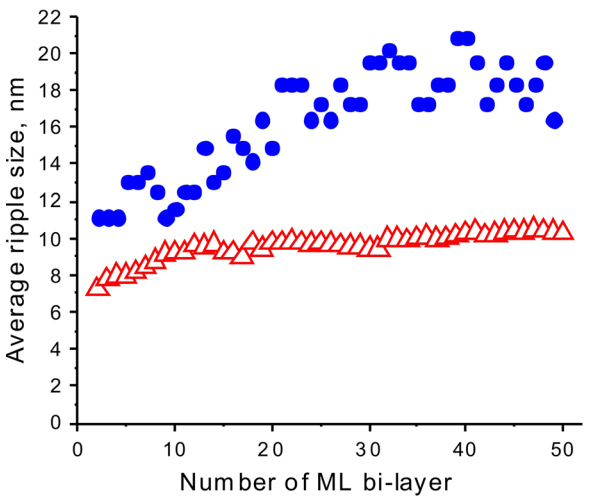

FIG. 8. Lateral width of the interface ripples as a function of the layer number for the Mo/Si multilayers deposited at angles of 55° (blue) and 65° (red).

resembles the columnar growth. However, the existing models for columnar growth cannot be applied to our multilayers which are grown under completely different conditions compared to those typical for normal columnar growth. Moreover, the observed structure of the multilayer stack is not consistent with the growth scenarios discussed in the literature for the columnar growth.[22–25]

Columnar growth is typically observed for films deposited by chemical vapor deposition (CVD), oblique angle deposition (OAD) and glancing angle deposition (GLAD), and sometimes by dc-magnetron sputtering. All these techniques often produce deposited particles of low energy and a certain portion of the particles impinge on the substrate surface at very small glancing angles.[26] For example, in the case of CVD, isotropic film growth occurs via decomposition of precursor gas molecules which arrive on the substrate surface from all possible directions. Magnetron sputtering generates particles of elevated energy which impinge on the substrate surface at different angles. Under nominal normal deposition conditions and low pressure of the sputtering gas, a relatively small number of atoms arrive at grazing angles on the substrate. However, if the sputtering is performed at an elevated pressure of the sputtering gas, trajectories of the sputtered particles can be altered by collisions with atoms of the noble gas, increasing the number of particles arriving at the substrate along significantly oblique directions. On the other hand, the collisional energy exchange results in thermalization of the sputtered atoms and they bring less energy to the growing surface, which results in low mobility of adatoms. OAD and GLAD are versions of low energetic sputtering or e-beam evaporation techniques when the glancing deposition is implemented by tilting a plane substrate with respect to the deposition flux. Due to the glancing component of deposition flux and the low mobility of adatoms, any small surface perturbations are picked up by shadowing which causes differences in growth rates for hills versus valleys. The shadowing produces areas that the deposited particles cannot directly reach, while adatom mobility is too low for surface diffusion to fill the voids. This results in dramatic enhancement of the roughness and separation of the continuous film into individual columns or pillars.[18–21]

The growth of multilayers in this work occurred under very different conditions. Although we deposited our multilayers at large angles (up to 65° from the normal), the high vacuum ion-beam sputtering setup (Fig. 1) provided tight control of the deposition angle for the collimated atomic flux, and the glancing component of deposition at the angles close to 90° is excluded. The second distinction is that average energy of the deposited particles was as high as 10 eV, which is approximately two orders of magnitude higher than for the deposition methods mentioned above. Deposition of the energetic particles is expected to promote intense surface diffusion. Under these conditions, the shadowing is very unlikely to happen in the very beginning of the multilayer growth when the film surface is very smooth. Due to the highly collimated deposition flux, the deposition angle variation did not exceed +/−7° at most. To produce shadowing at the deposition angle of 65°, the surface should have slope variations more than +/−18° which are not observed either in TEM [Figs. 5(a)–5(c)] or AFM [Figs. 2(a)–2(d)] images of the smooth multilayers. One still can speculate that the shadowing is caused by atomic size bumps (i.e., by ultra-high frequency defects which are not seen in the TEM and AFM images), but such ultra-high frequency surface features have low chances to survive and are expected to be smoothed out by the enhanced surface diffusion. Indeed, the PSD spectra of the normally deposited multilayer [black curve in Fig. 4(a)] show a suppression of spatial frequencies higher than 0.01 nm^{-1}. Based on the highly controlled deposition conditions, we can assume that shadowing was essentially not possible and hence could not serve as a dominating roughening mechanism in the beginning of the film growth.

Columnar growth models[18,22,24] assume some initial roughening which triggers the shadowing. Nucleation and 3D island growth according to the Volmer-Weber mechanism[27] can cause surface roughening at the very beginning of the film growth. Following growth, merging and coalescence of the islands result in the formation of continuous films with a relatively smooth surface. However, smoothing a rough surface is hardly possible for the oblique deposition when shadowing comes into play. The islands serve as shadow centers, and the surface roughness is picked up and enhanced by shadowing, preventing island merging. Under these conditions, a continuous film might never form, and the growth of isolated pillars is observed.[18,22] However, such a scenario is not consistent with the structure of the ion-beam sputtered multilayers revealed by TEM. For example, smooth top surface (interface #1) of the 1st continuous Mo layer in Fig. 7(c) apparently indicates that the stages of island growth, merging, and coalescence are over, but no evidence of shadowing is observed. The nucleation-caused roughness had not been picked up by the shadowing, and this allowed coalescence and smoothing of the top surface of the layer (interface #1). This supports our assumption that shadowing is not the dominant growth mechanism in the beginning of the multilayer growth and is overwhelmed by strong surface relaxation.

Despite the strong adatom mobility and the lack of shadowing, interface #2 of the 65° multilayer exhibits the formation of surface ripples which becomes more pronounced for interfaces #3 and #4 [Fig. 7(c)]. A subsequent growth of the ripple amplitude results in high surface slope variation, which causes the onset of shadowing. Thus, the shadowing is triggered by the ripples which had developed earlier from the almost ideally smooth surface. The structure of the multilayers deposited at lower angles is consistent with such a scenario. Indeed, the gradual development of the interface waviness in the bottom part [Fig. 7(a)] of the 55° deposited multilayer precedes shadowing apparent in the upper part [Fig. 6(a)]. Initial stages of ripple formation can also be noticed for the 45° deposited multilayer with no evident shadowing effects [Fig. 5(e)]. Summarizing this part, the deposition conditions and the experimental data indicate that shadowing was not a dominant growth mechanism in the beginning of the multilayer growth. It is very likely that formation of the ripples preceded the shadowing and slab formation, and an alternative roughening mechanism leading to periodic ripple formation should be considered.

B. Ripple growth model

The multilayers in this work were grown under conditions of strong surface relaxation, but nevertheless they exhibit strong roughening of the interfaces and periodical ripple patterns for oblique deposition. Here, we outline a preliminary model of ripple growth, which is consistent with the experimental results and can be a starting point for further experiments and theoretical investigations.

The growth of a variety of thin films including multilayers was found to be successfully described by continuous equations of motion.[16,17] According to the simplest growth models, the surface of the growing film undergoes stochastic roughening caused by time/space variations of the local deposition rate due to the random nature of the deposition flux. The stochastic roughening described by a Gaussian random variable with zero mean and shot-noise-type covariance, $\eta(x, t)$, results in the growth of roughness modes of all spatial frequencies with the film thickness. On the other hand, the surface roughness is suppressed by surface relaxation processes. Such growth is described by a continuum equation

$$\frac{\partial h(x,t)}{\partial t} = -B\frac{\partial^n}{\partial x^n}h(x,t) + \eta(x,t), \tag{1}$$

where n is a smoothing exponent, which ranges from 1 to 4 depending on the dominant relaxation mechanism such as surface diffusion, bulk diffusion, viscous flow, etc. For example, if surface diffusion is a primary lateral transport mechanism, the growth is described by the Wolf-Villian equation[28]

$$\frac{\partial h(x,t)}{\partial t} = -B\frac{\partial^4}{\partial x^4}h(x,t) + \eta(x,t). \tag{2}$$

Equation (2) with a smoothing exponent $n=4$ was found to work well for a variety of multilayers deposited by magnetron sputtering.[21,29] The growth conditions for those multilayers are characterized by the relatively high energy of the deposited particles, which promote isotropic surface diffusion. On the other hand, multilayers deposited by the ion-beam sputtering method often exhibit an additional relaxation process with the smoothing exponent $n=2$.[14,30] The energy of the landing atoms in such experiments is high enough to produce a substantial ballistic effect providing momentum transfer from the atoms to the surface. If a local area of the surface is tilted with respect to the deposition flux, the surface bombardment results in a directional drift of the material, the so-called downhill current. For a wavy surface, the downhill currents cause mass transfer from peaks to valleys and result in surface smoothing. Moseler *et al*. found by molecular dynamics simulations that the drift is proportional to the local surface tilt, ϕ, with respect to the normal deposition flux.[31] For small angles, they adopted $J_{curr.} \propto tg\phi = \partial h(x,t)/\partial x$ and concluded that the downhill current smoothing is described by the Edwards-Wilkinson equation

$$\frac{\partial h(x,t)}{\partial t} = B\frac{\partial^2}{\partial x^2}h(x,t) + \eta(x,t). \tag{3}$$

Solutions of Eqs. (1)–(3) lead to PSD spectra consisting of a frequency independent part at low frequencies and a frequency dependent fractal part with a $1/f^n$ slope defined by the relaxation exponent [see, for example, the black curve in Fig. 4(a)]. The growth rate of all surface modes with a wavelength longer than a correlation length is the same due to the frequency independent stochastic noise term, while the growth of higher frequency modes is suppressed by surface relaxation, and the slope part of the PSD curves does not change with the film thickness. None of the film growth Eqs. (1)–(3) leads to the ripple morphology and the respective PSD [red curve in Fig. 4(a)]. This is not surprising, since the models cover the growth of fairly smooth thin films and the ripples have not been observed so far on a surface of growing films. On the other hand, erosion of a surface under bombardment by energetic ions is well known to result in ripple formation. Indeed, some experimentally observed ripple patterns of the sputtered surfaces look very similar to those shown in Figs. 3(e) and 3(f) (see, for example, AFM images of a sputtered surface of Si in Refs. 32 and 33).

The ripple formation for ion sputtered surfaces is currently very well understood. According to the Bradly-Harper (BH) continuum model,[34] which incorporates the Sigmund theory for sputter yield,[35] the ion bombardment can cause surface instability resulting in roughening of the surface. The sputtering rate is proportional to the local surface curvature which results in the preferential sputtering of valleys as compared to bumps. On the other hand, surface diffusion causes short range smoothing of the surface. Following Ref. 33, the simplest linear continuum equation for the sputtered surface can be written as:

$$\frac{\partial h(x,t)}{\partial t} = S(\theta)K(x) - B\frac{\partial^2}{\partial x^2}K(x), \tag{4}$$

where S(θ) is the strength of the roughening process which depends on the incidence angle θ, K(x) is the local surface curvature, and B is the strength of the relaxation process. The second term represents the surface diffusion and is identical to the one in Eq. (2) for low surface roughness, where the surface curvature can be approximated as

$$K(x) \approx \frac{\partial^2 h(x,t)}{\partial x^2}.$$

Both the roughening and smoothing terms of Eq. (4) depend on the local surface curvature, and their impact increases with the spatial frequency. Due to the roughening term, surface modes of high frequency grow faster than low frequency modes. However, very high frequency features of the surface are effectively smoothed by surface diffusion which has a stronger dependence on the spatial frequency. As a result of the two competing processes, the surface mode of the fastest growing spatial frequency, $f_{res.} = (S/2B)^{1/2}$, dominates the surface leading to the periodic ripple morphology.

The BH model is valid for the high energy of the ions (typically, a few KeV)) which is not the case for this work. The energy of the Si and Mo atoms arriving at the substrate is too low to produce re-sputtering of the growing film (2

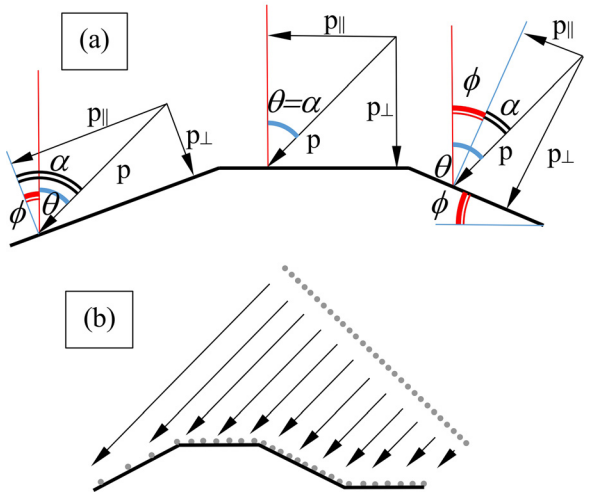

FIG. 9. Schematic of transfer of momentum of landing particles for inclined deposition. Tangential component of the projectile momentum which promotes surface diffusion current depends on both the global angle of deposition, θ, and the surface slope variation, ϕ, (a). Surface density of the deposited particles is also defined by θ and ϕ as schematically shown in (b).

orders of magnitude less than for the erosion experiments). Re-sputtering of the surface of the growing multilayer by recoiled Kr neutrals is also not likely since the probability of reflection of heavy Kr^+ ions from Si and Mo targets is vanishingly small.[14] Lack of re-sputtering of the multilayers is consistent with the deposition rates of Mo and Si following the simple cosine law with the deposition angle (Fig. 2). Although the BH model is not applicable for the ML growth, the principle of competition between the roughening and smoothing processes resulting in the preferential growth of the resonance frequency mode can be adopted for a growing film surface. The frequency dependent roughening term is a key for the ripple formation mechanism for sputtered surfaces. A similar frequency dependent roughening mechanism corresponding to the ML growth conditions should be found.

As was mentioned above, we can expect a strong promoted diffusion for the ion-beam sputtered multilayers. For the normal deposition geometry when the deposition flux is perpendicular to the growing surface, the diffusion results in effective smoothing of surface imperfections. However, the situation might change dramatically for deposition at some angle, θ, between the deposition flux and the global surface normal. For the inclined deposition, the momentum of incoming particles has normal and tangential components which depend on the local deposition angle, α, (see Fig. 9)

$$p_{\parallel} = p\sin\alpha,$$
$$p_{\perp} = p\cos\alpha,$$
$$\alpha = \theta + \phi,$$

where ϕ is the local tilt angle of the surface $h(x,t)$ and can be found as $tg\phi = \partial h(x,t)/\partial x$.

The normal component of the momentum, $p_{\perp}$, which is perpendicular to the local surface, being transferred to the surface atoms promotes isotropic diffusion driven by a local surface curvature; this process is described by the first term of Eq. (2). The tangential component of the momentum promotes a directed surface flux along the surface (although a part of the tangential momentum probably dissipates isotopically due to collisions of the projectile with the surface atoms contributing to the isotropic diffusion flux). For the normal deposition, this is essentially the mechanism of downhill currents, but for substantially oblique angles ($\theta > \phi$), the direction of the surface flux is the same for the opposite slopes of a surface hill and hence includes both downhill and uphill currents now. In this way, there is a global surface current directed along the projection of the deposition flux on the substrate. It is natural to assume that the directed flux is proportional to the tangential component of the projectile momentum, $J_{\text{dir.}} \propto p\sin\alpha$. On the other hand, the promoted surface flux is proportional to the quantity of the mobile (promoted) surface atoms. The surface concentration, c_α, of the promoted species depends on the number of projectiles, N, landing per unit area, s, [see Fig. 9(b)]

$$c_\alpha = \frac{N}{s} = c_0\cos\alpha,$$

where c_0 is the concentration of the particles in the deposition flux. In terms of both geometrical effects, one can write: $J_{dir.} \propto p_{\parallel} \times c_\alpha$. The resulting surface current

$$J_{dir.} = -A\sin\alpha\cos\alpha = -\frac{A}{2}\sin 2\alpha, \tag{5}$$

where A is a strength parameter which characterizes the efficiency of momentum transfer. In our simple model, we assume that parameter A is constant and does not depend on the angle. The minus sign corresponds to the direction of the current opposite to the x axis in Fig. 9. Note that for normal deposition ($\theta = 0°$) and for a relatively smooth surface ($\phi \to 0$), the expression (5) for the flux reduces to $J_{dir.} \propto \sin\phi$, which is almost identical to $J \propto tg\phi$, adopted by Moseler *et al.* for the downhill current model.[31] In that sense, Eq. (5) is an extension of the downhill current model for oblique deposition.

For ideally smooth surfaces ($\phi = 0$), the directed flux is uniform and does not affect the surface. If the surface is not ideally smooth, the local slope variation causes a variation of the local deposition angle and results in non-uniform surface current according to Eq. (5). This results in redistribution of the material along the surface and a non-uniform surface growth rate depending on the local deposition angle

$$\frac{\partial h(x,t)}{\partial t} = -divJ_{dir.} = \frac{\partial}{\partial x}\left(\frac{A}{2}\sin 2\alpha\right) = A\cos 2\alpha\frac{\partial\alpha}{\partial x}. \tag{6}$$

Formula (6) describes the increment of a surface with deposition time. To show the evolution of the surface with the film thickness, the cosine law should be taken into account. Since the average thickness, z, of the deposited film is proportional to the deposition time and depends on the angle of deposition as $\partial z \propto \partial t\cos\theta$, Eq. (6) can be modified as

$$\frac{\partial h(x,z)}{\partial z} = \frac{A}{\cos\theta}\cos 2\alpha(x)\frac{\partial\alpha(x)}{\partial x}. \tag{7}$$

Taking into account $\alpha = \theta + \phi$, formula (6) can be modified as

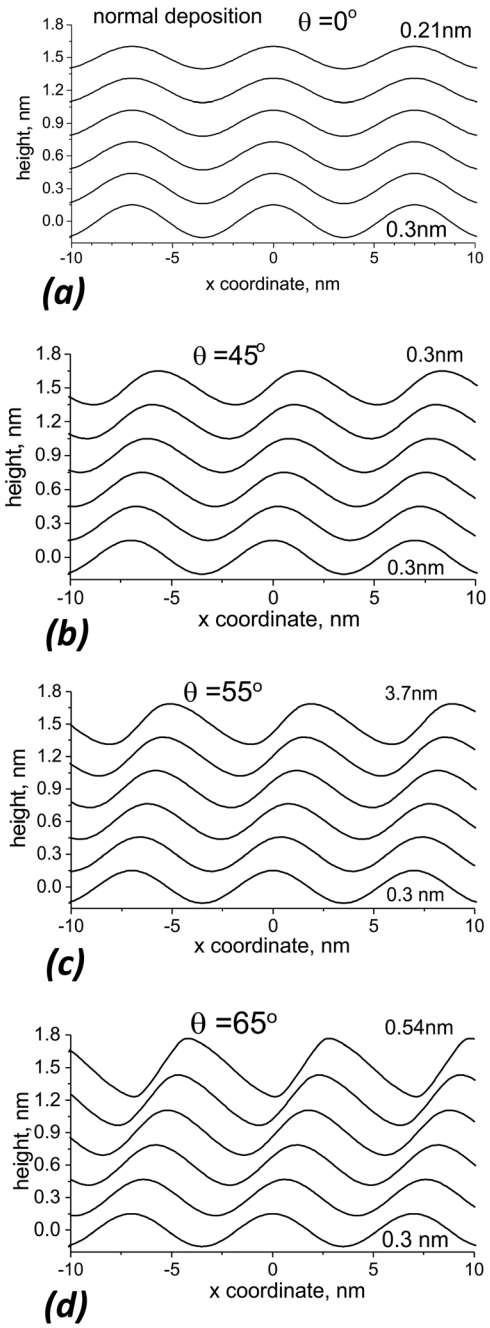

FIG. 10. Evolution of a sinusoidal surface due to the directed surface flux according to Eq. (7) for normal deposition (a) and the deposition angles of 45°, 55° and 65° [(b)–(d)].

$$\frac{\partial h(x,t)}{\partial t} = A\cos 2\alpha \frac{\partial(\theta+\phi)}{\partial x} = A\cos 2\alpha \frac{\partial \phi}{\partial x}.$$

For a surface of very low roughness $\phi \to 0$ and $\phi \approx tg\phi = \partial h(x,t)/\partial x$, and for some deposition angle $\theta \gg \phi$, the formula reduces to

$$\frac{\partial h(x,t)}{\partial t} = A\cos 2\theta \frac{\partial^2 h(x,t)}{\partial x^2}. \quad (8)$$

For normal deposition ($\theta = 0°$), the right part of Eq. (8) converges to the smoothing term of the Edwards-Wilkinson continuum equation [see Eq. (3)] corresponding to Moseler's downhill current model.[31] However, formula (8) shows that the strength of the smoothing process reduces with the deposition angle as $\cos 2\theta$ and reaches zero for $\theta = 45°$. This means that the directed surface current does not affect the surface relief at all for the deposition angle of 45°. For more oblique deposition ($\theta > 45°$), the right part of Eq. (8) changes its sign due to the cosine factor and turns into the roughening term of Eq. (4) implying transition from a smoothing to a roughening regime.

The impact of the promoted surface diffusion described by Eq. (7) on a surface with initially sinusoidal profile is illustrated in Fig. 10 for different deposition angles. The spatial wavelength of 7 nm and the initial amplitude of 0.3 nm of the sinusoidal surface are consistent with parameters of the highest frequency modes of random roughness observed in the AFM images [see the inset in Fig. 3(a)]. Simulation of the film growth using Eq. (7) shows that the amplitude of the sinusoidal surface gradually decays with the thickness of the coating [Fig. 10(a)] for the normal deposition conditions, meaning smoothing of the surface. The smoothing effect diminishes with the angle of deposition and goes to zero for angles around 45° [Fig. 10(b)]. For the angle of 55°, the amplitude of the profile increases with the film thickness [Fig. 10(c)], meaning roughening of the surface. More oblique deposition results in faster growth of the amplitude [Fig. 10(d)] indicating that the strength of the roughening increases with the angle of deposition.

The fact that a diffusion process results in roughening of a surface is very unusual and may seem self-contradictory. Note, however, that the promoted surface current is not a regular diffusion mass transfer process driven by a gradient of chemical potential which depends on the surface curvature. The regular surface diffusion flux is directed against the gradient and results in a reduction of the gradient of chemical potential by surface smoothing. In contrast to that, the promoted surface current is a solely ballistic effect of momentum transfer, which depends on a local angle of deposition [see Eq. (5)] and does not depend on the chemical potential. A direction of the promoted surface flux is defined by the deposition direction and a local surface tilt, and might be either against or along the gradient of chemical potential resulting in surface smoothing or roughening, respectively. A similar smoothing process was observed by Garter and Vishniakov (CV) for sputtering of a Si surface by 10–40 KeV Xe^+ ions in the angle range of 0–45°.[36] The momentum transfer from the ions to the target induces a diffusion of atoms in a surface layer of a certain thickness defined by the penetration depth of the ions. Although the CV model describes a volume transport rather than surface diffusion, the induced flux has the same angular dependence and causes a smoothing effect at moderate angles of sputtering, preventing the ripple formation.[36] The bulk current is expected to produce ripples at angles larger than 45°,[37] though it can hardly be distinguished from the BH effect in a sputtering experiment.

Simulations performed using Eq. (7) for sinusoidal surfaces of different wavelengths showed that the strength of both smoothing and roughening regimes strongly depends on spatial frequency. The amplitude of sinusoidal profiles with

the same initial amplitude of 0.3 nm, but different spatial wavelengths in the range of 4–100 nm after deposition of a 1.5 nm thick film at different angles is shown in Fig. 11. While low frequency modes are almost unaffected by the surface current, the high frequency modes are effectively suppressed for low angle deposition ($\theta < 45°$) and dramatically enhanced at the substantially oblique deposition angles ($\theta > 45°$).

The directed surface current is caused by surface adatoms which inherited at least partially the momentum of the deposited projectiles. At the same time, multiple surface collisions result in thermalization of the initial momentum and generate a number of mobile adatoms which move in all directions. These particles contribute to the isotropic component of the promoted surface diffusion, which is characterized by the smoothing exponent $n = 4$ [see Eq. (2)]. The other contribution to the isotropic diffusion comes from the normal component of the momentum $p_\perp$ of the deposited particles. Since both smoothing mechanisms with $n = 2$ and $n = 4$ are observed for ion-beam sputtered multilayers,[14,30] the isotropic surface diffusion term should be added in Eq. (7) along with the noise term, so the final continuum equation can be composed as

$$\frac{\partial h(x,z)}{\partial z} = \frac{A}{\cos\theta}\cos 2\alpha(x)\frac{\partial \alpha(x)}{\partial x} - B\frac{\partial^2}{\partial x^2}K(x) + \eta(x,z). \quad (9)$$

Based on Eq. (9), one can outline the following scenario for ripple formation. For the normal and moderately inclined deposition, both the 1st and 2nd terms in the right part of Eq. (9) provide smoothing of the random roughness of the substrate surface and the random film roughness caused by the 3rd term. However, at sufficiently oblique deposition, the directed surface current described by the 1st term in Eq. (8) results in roughening rather than smoothing. While the noise term causes surface height variations of all frequencies, the high frequency modes are picked up and enhanced by the non-uniform surface current. At the same time, the roughening is counterbalanced at the highest frequencies by the isotropic diffusion term. This term is known to be strongly dependent on spatial frequency (as f^4) and dominates all other processes at very high frequencies. Competition between the two frequency dependent processes results in predominant growth of a single resonance frequency mode with the highest net growth rate, while other modes are substantially suppressed. This results in the formation of surface ripples of a very distinct resonance wavelength similar to the ripples obtained on the surfaces eroded by ion sputtering.

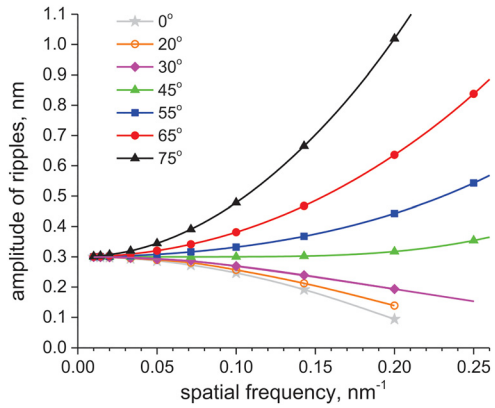

FIG. 11. Dependence of the amplitude of sinusoidal surfaces on the spatial frequency for different angles of deposition.

The value of the resonance frequency is defined by a balance of impacts of the directed and isotropic diffusion fluxes. Since both processes are promoted by the bombardment and depend on $p_{||}$ and $p_\perp$, respectively, the impact of the 1st term increases with the angle, while the second term reduces, which can shift the balance towards shorter wavelengths. For the higher deposition angle, the higher frequency modes can survive against smoothing, and hence the shorter period ripples can form as observed for the 55° and 65° multilayers.

The roughening term [Eq. (8)] is anisotropic and amplifies the roughness in the direction of the surface flux. In the transverse direction, roughening is caused by the noise term only and it is smoothed out by the isotropic term of the promoted diffusion. This results in ripples oriented perpendicular to the flux direction.

As the amplitude of the ripples increases and the local surface slope exceeds the deposition angle $\phi > \theta$, the shadowing takes effect (from this moment, the continuum approach is not applicable anymore) resulting in partitioning of the continuous film into separated slabs. Due to high periodicity of the ripples, the slabs are almost of the same width and height and have equal chances of survival, and further deposition results in only a marginal change in the ripple shape and wavelength coarsening. The random component of kinetic roughening of the surface reflected on the PSD spectra as a vertical shift of the curves for the 65° sample as compared to the normally deposited multilayer is probably caused by the residual spread of the slab width. Indeed, the local thickness, $H(x)$, of the coating which consists of slanted slabs is

$$H(x) = \sum_k w_k / tg\varphi,$$

where w_k is the slab width, k is the number of slabs above a particular point x, and φ is the slab tilt angle. Since the column width varies randomly, the top surface height variation is proportional to the square root of the number of slabs above the local position. If so, the random roughness is expected to grow with the total multilayer thickness as $\sigma \propto \sqrt{H}$.

As was mentioned earlier, the directed surface flux does not substantially affect the amplitude of Fourier modes of different frequencies at deposition angles around 45° (Fig. 11). This means that the growth of a film on a sculptured surface should not change the surface relief. This regime seems very promising for the multilayer blazed grating applications where replication of the saw-tooth substrate profile by the multilayer interfaces is of great important since smoothing of the profile results in degradation of the diffraction efficiency of MBGs.[38]

V. SUMMARY

We investigated the growth of ion-beam sputtered Mo/Si multilayers in a wide range of deposition angles and

discovered a new regime of multilayer growth resulting in highly periodic lateral ripple patterns. We present a simple model of ripple formation that assumes that promoted surface diffusion causes smoothing of interfaces at small angles, but results in roughening of the interfaces at substantially oblique deposition.

Bombardment of the surface of the growing multilayer by energetic atoms generated by ion-beam sputtering promotes adatom mobility and enhanced surface diffusion which is isotropic for normal deposition. In contrast, inclined deposition results in a directed surface diffusion current due to the transfer of momentum of the landing particles to surface atoms. The momentum transfer depends on the local deposition angle, which is defined by the global deposition angle and a local surface tilt. For a random surface with some initial slope variations, the bombardment results in a non-uniform surface current leading to redistribution of materials along the surface. For small angles, the surface current causes a smoothing effect which, however, diminishes as the angle of deposition approaches 45°. This regime is very promising for the growth of films on sculptured surfaces such as multilayer blazed gratings, since it provides perfect replication of a substrate by the multilayer interfaces. For more oblique deposition, the non-uniform surface current has a reverse effect resulting in roughening of the surface. The impact of the roughening increases with the spatial frequency resulting in a fast growth of high-frequency modes. Competition of the directed flux roughening with the isotropic diffusion component of the surface relaxation results in selective enhancement of a resonance frequency mode leading to ripple formation. Due to high lateral periodicity of the ripples and vertical periodicity of the multilayer, the obliquely deposited coating consists of Mo and Si nanowires closely packed into a 6-fold symmetry array. This effect might be useful for the synthesis of a variety of nanostructures that could be used in a wide range of applications. For example, magnetic nanowires with a high degree of anisotropy might be useful as magnetic storage elements.

ACKNOWLEDGMENTS

Advanced Light Source and Molecular Foundry are supported by the Director, Office of Science, Office of Basic Energy Sciences, the U.S. Department of Energy under Contract No. DE-AC02-05CH11231.

This document was prepared as an account of work sponsored by the United States Government. While this document is believed to contain correct information, neither the United States Government nor any agency thereof, nor The Regents of the University of California, nor any of their employees, make any warranty, express or imply, or assume any legal responsibility for the accuracy, completeness, or usefulness of any information, apparatus, product, or process disclosed, or represent that its use would not infringe privately owned rights. Reference herein to any specific commercial product, process, or service by its trade name, trademark, manufacturer, or otherwise, does not necessarily constitute or imply its endorsement, recommendation, or favoring by the United States Government or any agency thereof, or The Regents of the University of California. The views and opinions of authors expressed herein do not necessarily state or reflect those of the United States Government or any agency thereof or The Regents of the University of California.

[1]R. Soufli, IEEE Photonics J. **6**, 0700606 (2014).
[2]E. Louis, A. E. Yakshin, T. Tsarfati, and F. Bijkerk, Prog. Surf. Sci. **86**, 255 (2011).
[3]R. M. Bionta, A. Ables, O. Clamp, O. D. Edwards, P. C. Gabriele, K. Miller, L. L. Ott, K. M. Skulina, R. Tilley, and Y. Viada, Opt. Eng. **29**, 576 (1990).
[4]F. Doring, A. L. Robisch, C. Eberl, M. Osterhoff, A. Ruhlandt, T. Liese, F. Schlenkrich, S. Hoffmann, M. Bartels, T. Salditt, and H. U. Krebs, Opt. Express **21**, 19311 (2013).
[5]F. X. Huang, H. Yan, E. Nazaretski, R. Conley, N. Bouet, J. Zhou, K. Lauer, L. Li, D. Eom, D. Legnini, R. Harder, I. K. Robinson, and Y. S. Chu, Sci. Rep. **3**, 3562 (2013).
[6]N. I. Chkhalo, M. N. Drozdov, E. B. Kluenkov, A. Ya. Lopatin, V. I. Luchin, N. N. Salashchenko, N. N. Tsybin, L. A. Sjmaenok, V. E. Banine, and A. M. Yakunin, J. Micro/Nanolithogr. MEMS MOEMS **11**, 021115 (2012).
[7]V. V. Medvedev, A. J. R. van den Boogaard, R. van der Meer, A. E. Yakshin, E. Louis, V. M. Krivtsun, and F. Bijkerk, Opt. Express **21**, 16964 (2013).
[8]B. Lagarde, F. Choueikani, B. Capitanio, P. Ohresser, E. Meltchakov, F. Delmotte, M. Krumrey, and F. Polack, J. Phys. Conf. Ser. **425**, 152012 (2013).
[9]F. Senf, F. Bijkerk, F. Eggenstein, G. Gwalt, Q. Huang, R. Kruijs, O. Kutz, S. Lemke, E. Louis, M. Mertin, I. Packe, I. Rudolph, F. Schäfers, F. Siewert, A. Sokolov, J. M. Sturm, Ch. Waberski, Z. Wang, J. Wolf, T. Zeschke, and A. Erko, Opt. Express **24**, 13220 (2016).
[10]D. L. Voronov, F. Salmassi, J. Meyer-Ilse, E. M. Gullikson, T. Warwick, and H. A. Padmore, Opt. Express **24**, 11334 (2016).
[11]M. Bayraktar, F. A. van Goor, K. J. Boller, and F. Bijkerk, Opt. Express **22**, 8633 (2014).
[12]S. K. Lynch, C. Liu, N. Y. Morgan, X. Xiao, A. A. Gomella, D. Mazilu, E. E. Bennett, L. Assoufid, F. de Carlo, and H. Wen, J. Micromech. Microeng. **22**, 105007 (2012).
[13]M. Prasciolu, A. Haase, F. Scholze, H. N. Chapman, and S. Bajt, Opt. Express **23**, 15195 (2015).
[14]D. L. Voronov, P. Gawlitza, R. Cambie, S. Dhuey, E. M. Gullikson, T. Warwick, S. Braun, V. V. Yashchuk, and H. A. Padmore, J. Appl. Phys. **111**, 093521 (2012).
[15]J. Villain, J. Phys. I France **1**, 19 (1991).
[16]W. M. Tong and R. S. Williams, Annu. Rev. Phys. Chem. **45**, 401 (1994).
[17]Y. Cheng, D. J. Smith, M. B. Stearns, and D. G. Stearns, J. Appl. Phys. **72**, 5165 (1992).
[18]M. M. Hawkeye and M. J. Brett, J. Vac. Sci. Technol. A **25**, 1317 (2007).
[19]S. P. Vernon, D. G. Stearns, and R. S. Rosen, Appl. Opt. **32**, 6969 (1993).
[20]T. Karabacak, Y.-P. Zhao, G.-C. Wang, and T.-M. Lu, Phys. Rev. B **64**, 085323 (2001).
[21]D. L. Voronov, E. H. Anderson, E. M. Gullikson, F. Salmassi, T. Warwick, V. V. Yashchuk, and H. A. Padmore, Appl. Surf. Sci. **284**, 575 (2013).
[22]K. Robbie and M. J. Brett, J. Vac. Sci. Technol. A **15**, 1460 (1997).
[23]A. G. Dirks and H. J. Leamy, Thin Solid Films **47**, 219 (1977).
[24]R. P. U. Karunasiri, R. Bruinsma, and J. Rudnick, Phys. Rev. Lett. **62**, 788 (1989).
[25]C. Tang, S. Alexander, and R. Bruinsma, Phys. Rev. Lett. **64**, 772 (1990).
[26]T. Karabacak, J. Nanophotonics **5**, 052501 (2011).
[27]M. Volmer and A. Weber, Z. Phys. Chem. **119**, 277 (1926).
[28]D. E. Wolf and J. Villain, "Growth with surface diffusion," Europhys. Lett. **13**, 389 (1990).
[29]D. G. Stearns, D. P. Gaines, D. W. Sweeney, and E. M. Gullikson, J. Appl. Phys. **84**, 1003 (1998).
[30]E. Spiller, S. Baker, E. Parra, and C. Tarrio, Proc. SPIE **3767**, 143 (1999).
[31]M. Moseler, P. Gumbsch, C. Casiraghi, A. C. Ferrari, and J. Robertson, Science **309**, 1545 (2005).
[32]A. Keller, R. Cuerno, S. Facsko, and W. Möller, Phys. Rev. B **79**, 115437 (2009).
[33]J. Erlebacher, M. J. Aziz, E. Chason, M. B. Sinclair, and J. A. Floro, Phys. Rev. Lett. **82**, 2330 (1999).

[34]R. M. Bradley and J. M. E. Harper, J. Vac. Sci. Technol. A **6**, 2390 (1988).
[35]P. Sigmund, J. Mater. Sci. **8**, 1545 (1973).
[36]G. Carter and V. Vishnyakov, "Roughening and ripple instabilities on ion-bombarded Si," Phys. Rev. B **54**, 17647 (1996).
[37]B. Davidovitch, M. J. Aziz, and M. P. Brenne, "On the stabilization of ion sputtered surfaces," Phys. Rev. B **76**, 205420 (2007).
[38]D. L. Voronov, E. H. Anderson, R. Cambie, S. Cabrini, S. D. Dhuey, L. I. Goray, E. M. Gullikson, F. Salmassi, T. Warwick, V. V. Yashchuk, and H. A. Padmore, Opt. Express **19**, 6320 (2011).